Analysis of the 2D Ising Model of a Ferromagnet Implemented via the Metropolis Algorithm

Lucas Strange

May 2, 2021

Abstract

A 2D Ising Model of a ferromagnet was implemented with a Metropolis algorithm and a second-order phase transition was observed through the magnetisation. The critical transition temperature, T_c, for an infinite sized lattice in the absence of an applied field was estimated from finite scaling. This was found to be $T_c = 2.275 \pm 0.006$, in agreement with Onsager's exact result of $T_c = \frac{2}{\ln(1+\sqrt{2})} \approx 2.269$. The proportionality constant of the finite scaling equation, a, was calculated to be $a = 1.26 \pm 0.06$. Our simulations were also in agreement with exact results calculated directly from the partition function. At T close to zero, metastable striped states were reached approximately 3/10 of the time, while the ground state was reached otherwise. The lifetime of these striped states were a barrier towards averaging observables, and solutions in the form of a low quench from $T = (\infty \to 0)$ and next-to-nearest neighbour interaction were suggested. Applying an oscillating magnetic field led to the formation of hysteresis loops. The shapes, areas and coercive fields of the hysteresis loops were studied as function of temperature and amplitude.

1 Introduction

Ferromagnetism is the mechanism by which certain materials, e.g. iron, exhibit a macroscopic magnetic moment below a certain temperature, called the *Curie temperature*, due to the alignment of atomic spins. Above the Curie temperature, these spins become randomly orientated and we observe a phase transition through the abrupt change of the overall magnetic moment. A full description of the system would require a quantum mechanical analysis of spin. The Ising model removes unnecessary complexity from ferromagnetism and provides a mathematically tractable, classical description whilst still retaining the essential physics. Implementing a $2D$ Ising Model via the Metropolis algorithm, the properties of a ferromagnet were investigated. Observations of the time to reach equilibrium were made, in particular at the low temperature limit, where metastable states become problematic. The energy, magnetisation, specific heat capacity and magnetic susceptibility were computed as functions of temperature for varying lattice sizes. A phase transition was illustrated and the critical temperature T_c was found for differing lattice sizes, from which we obtain an estimate of $T_c(\infty)$ via finite scaling. Finally, the effect of an applied oscillating magnetic field at varying temperatures was investigated. The results obtained throughout were compared to exact calculations to support the validity of this numerical process.

2 Analysis

2.1 Ising Model

The $2D$ Ising model treats a ferromagnet as a lattice with a spin s_i at each site i , such that $s_i = +1$ or -1 for up ($\uparrow$) or down ($\downarrow$) spins respectively. Figure 1 shows a schematic representation of this lattice. In this report we considered $N \times N$ square lattices, for a total of N^2 spins. For nearest neighbour interactions, the total energy E of the system is given by

$$E = -J \sum_{<ij>} s_i s_j - \mu H \sum_{i=1}^{N^2} s_i \tag{1}$$

where the sum $< ij >$ is over nearest neighbour pairs of atoms only. J is the interaction coupling constant, μ the magnetic moment and H the applied field. In the absence of an external magnetic field this becomes

$$E = -\frac{J}{2}\sum_{i,i+\delta} s_i s_j \tag{2}$$

such that the i sum runs over all sites in the lattice and the δ sum runs over the nearest neighbours. The factor of $1/2$ arises to avoid double counting. For $J > 0$, the spins energetically desire to be aligned and result in ferromagnetic properties. In our discussion set $J = k_B = \mu = 1$. The magnetisation M, specific heat capacity C and magnetic susceptibility χ are [6]:

$$M = \sum_{i=1}^{N^2} s_i \tag{3}$$

$$C = \frac{\langle E^2\rangle - \langle E\rangle^2}{T^2} \tag{4}$$

$$\chi = \frac{\langle M^2\rangle - \langle M\rangle^2}{T} \tag{5}$$

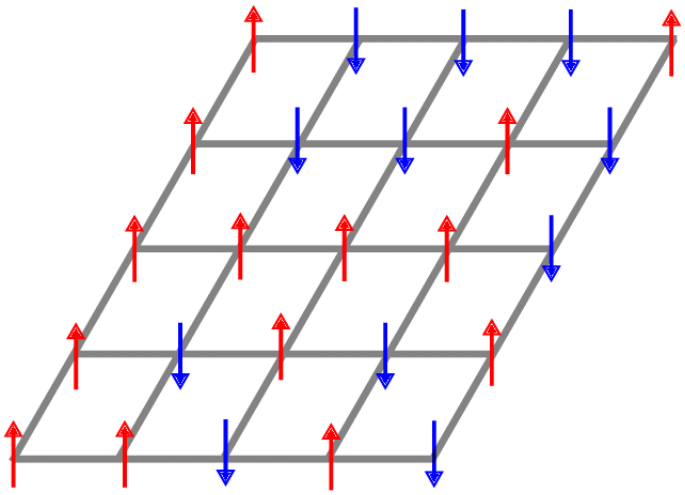

Figure 1: Schematic representation of a configuration of the 2D Ising model on a square lattice [16].

Period boundary conditions were employed to ensure every spin has four nearest neighbours, i.e. spins on the edge of the lattice interact with the spins on the geometrically opposite edge. This is equivalent to wrapping our $2D$ lattice on the surface of a $3D$ torus, as illustrated in Figure 2.

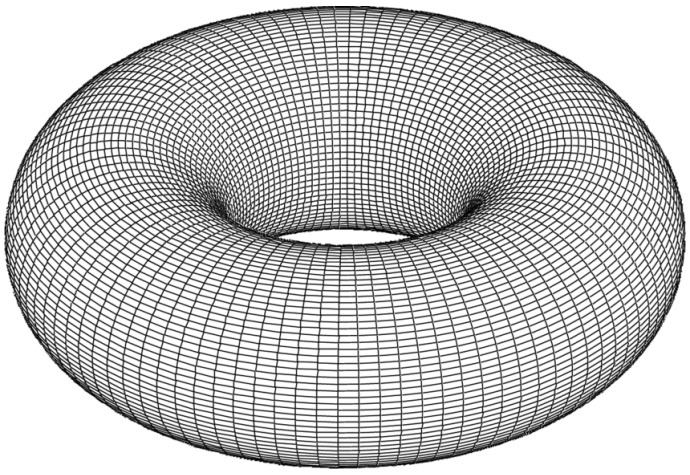

Figure 2: An illustration of a 100×100 lattice on the surface of a $3D$ torus. This is representative of a 100×100 lattice with with periodic boundary conditions [4].

Whilst a configuration with all its spins aligned would minimize the energy, it isn't necessarily the realized state. Assuming a rigid lattice, equilibrium is determined by minimizing the Helmholtz free energy

$$F = U - TS \tag{6}$$

At low temperatures, F is dominated by U, so minimizing U with an aligned lattice is favoured. On the other hand at high temperatures, F is dominated by $-TS$, so a disordered lattice that maximises entropy is preferred.

2.2 Exact Solutions and Scalability

The probability for a system in contact with a reservoir to be in a given microstate α is

$$p(\alpha) = \frac{e^{-\beta E(\alpha)}}{Z} \tag{7}$$

where $Z = \sum_\alpha e^{-E(\alpha)/k_b T}$ is the partition function. It then follows that for an observable $Q(\alpha)$, the thermal average is

$$\langle Q \rangle = \sum_\alpha Q(\alpha) p(\alpha) \tag{8}$$

For a 2×2 lattice, with 16 microstates, the average energy and absolute magnetisation per spin $\langle |m| \rangle$ can be directly calculated [6]

$$\langle E \rangle = -\frac{8 \sinh(8/T)}{3 + \cosh(8/T)} \tag{9}$$

$$\langle |m| \rangle = -\frac{2e^{8/T} + 4}{3 + \cosh(8/T)} \tag{10}$$

This calculation is manageable for small systems, but the number of distinct configurations on a $N \times N$ lattice, 2^{N^2}, grows very rapidly with N, as shown in Table 1. The vast number of microstates involved motivates us to simulate the Ising model using Monte-Carlo methods.

N	N^2	2^{N^2}
2	4	16
3	9	512
4	16	65,536
5	25	33,554,432
6	36	68,719,476,736
⋮	⋮	⋮

Table 1: The factor of 2^{N^2} grows very rapidly with N

Despite its apparent complications, exact solutions for the $2D$ square lattice Ising Model (but not $3D$) exist. As $N \to \infty$, the critical temperature was proved by Onsager in 1944 to be $T_c = \frac{2}{\ln(1+\sqrt{2})}$ [11]. In addition, stated by Onsager in 1948 and subsequently proved by C. N. Yang in 1952, the exact result of the spontaneous magnetisation is given by [9]

$$m = [1 - \sinh^{-4}(\frac{2}{T})]^{\frac{1}{8}} \tag{11}$$

"Finite size-scaling" suggests the relation between T_c at infinite and finite lattice sizes is given by

$$T_c(N) = T_c(\infty) + aN^{-1/\nu} \tag{12}$$

where a is a constant and ν is the critical exponent for correlation length [7].

2.3 Monte-Carlo Method

The basic idea behind a Monte Carlo method is to simulate the random thermal fluctuation of the system. As we pass through a variety of configurations, we desire to generate a random set of states according to the Boltzmann probability distribution- calculation of an expectation value then becomes time average over the states that a system passes through. The advantage of this technique is that we need only sample a small fraction of the states of the system in order to get accurate estimates of physical quantities. For example, we do not need to include every state of the system in order to get a decent value for the partition function. Almost all Monte Carlo schemes rely on Markov processes as the generating engine for the set of states used [10]. This is a mechanism which, given a system in one state μ, randomly generates a new state of that system ν with transition probability $P(\mu \to \nu)$. By feeding ν back into the process, a Markov chain of states is generated. The algorithm has satisfy the conditions of "ergodicity", which is achieved by single-spin-flip dynamics, and the "detailed balance" equation

$$p(\mu)P(\mu \to \nu) = p(\nu)P(\nu \to \mu) \tag{13}$$

Eq. (13) simply put is the condition that the rate at which the system makes transitions into and out of any state must be equal. If we take the ratio of the transition probabilities, we see that a move $\mu \to \nu$ and its inverse are only dependent on the the energy change

$$\frac{P(\mu \to \nu)}{P(\nu \to \mu)} = e^{-\beta(E_\nu - E_\mu)} \tag{14}$$

However, this doesn't determine $P(\mu \to \nu)$ uniquely. What characterizes the Metropolis algorithm is the specification of the transition probabilities as

$$P(\mu \to \nu) = \begin{cases} e^{-\beta(E_\nu - E_\mu)} & \text{if } E_\nu - E_\mu > 0 \\ 1 & \text{otherwise} \end{cases} \tag{15}$$

This specific choice, that correctly samples the Boltzmann distribution, is optimal compared to alternative routines matching the conditions of ergodicity and Eq. (13) [10].

3 Implementation

In this simulation, the steps of the Metropolis algorithm, illustrated in Figure 3, were as follows:

1. The temperature, initial square lattice ($N \times N$) and number of Monte-Carlo steps (MCs) are taken as an input
2. A list of integers from 0 to $N^2 - 1$ is generated and randomly shuffled. By using the floor and modulo functions, a list of sites on the lattice in random order is created.
3. Looping through all the elements in the list once, all N^2 spins are selected in random order.
4. When a given site is selected, a value for ΔE is obtained from Table 2. Based on ΔE a decision is made:
   - If $\Delta E \leq 0$, flip the spin at the selected site (e.g. a value of -1 $\to$ 1), update the lattice and E.
   - If $\Delta E > 0$, generate a random number. If this random number is $< \exp(\frac{-\Delta E}{k_b T})$, also obtained from Table 2, flip the spin at the selected site, update the lattice and E.
   - Else, do nothing.
5. Once all the sites have been visited, this constitutes a single time step. A copy of the lattice and its E in this state are stored.
6. Repeat steps $2 - 5$ for the input number of MCs, using the end lattice from the previous step as the initial input. The first step in the algorithm doesn't flip any of the spins but is instead used to calculate the initial energy E_I via Eq. (2)
7. The final outputs are sets of the lattice state and E after each MCs.

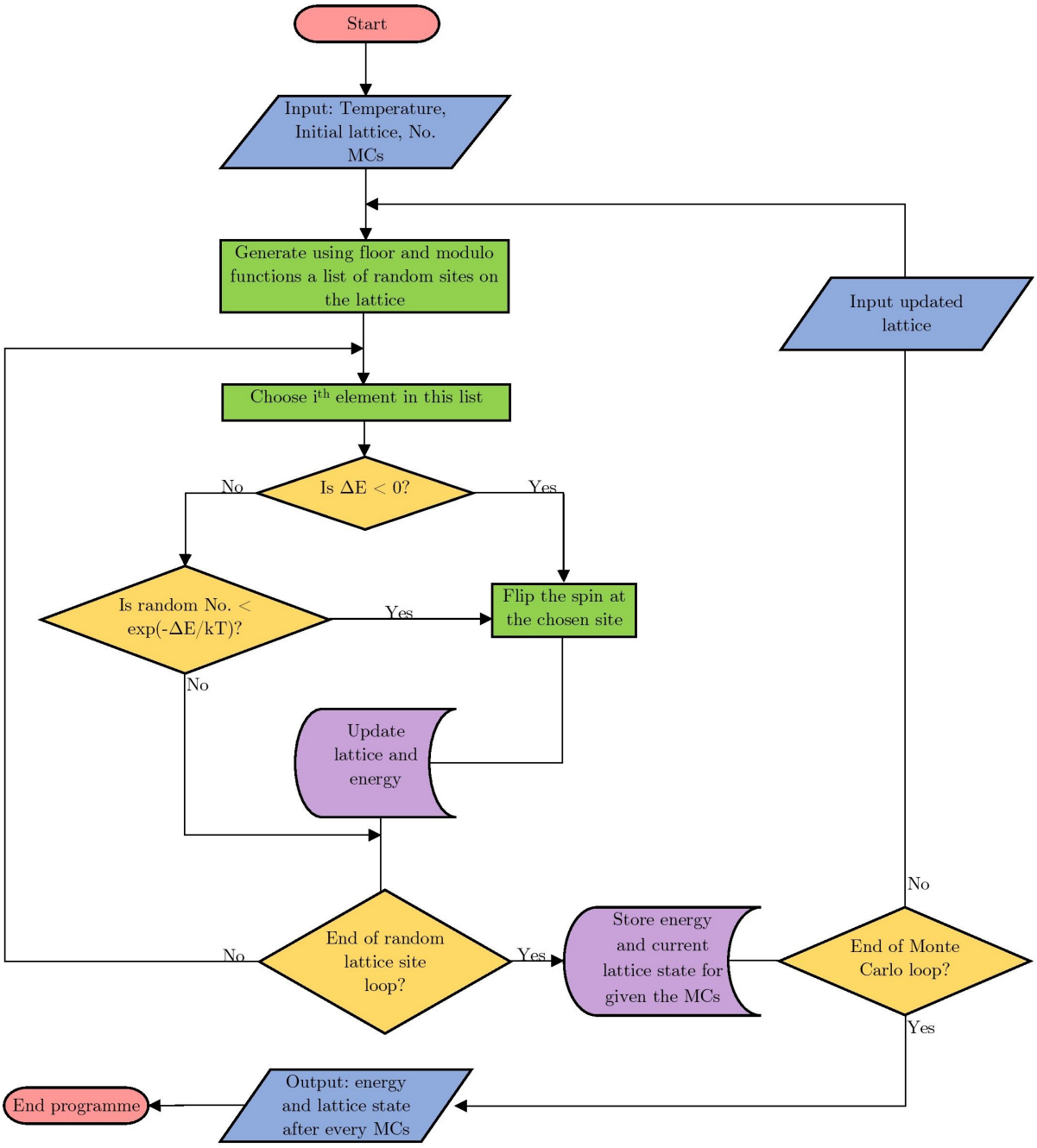

Figure 3: Flowchart of Metropolis Algorithm implemented in this simulation

The observables of interest were $\langle E\rangle, \langle E^2\rangle, \langle m\rangle, \langle |m|\rangle$ and $\langle m^2\rangle$, from which we obtained C, χ and the autocovariance $A(\tau)$. The calculation for E occured within the Metropolis algorithm; the initial energy E_I was obtained, and as each site was visited, the value of ΔE from Table 2 was added if the spin is flipped. Thus the total energy at a given MCs became

$$E = E_I + \sum_{j=1}^{No.MCs} \sum_{i=1}^{N^2} \Delta E_i \tag{16}$$

with $\Delta E_i = 0$ if the spin is unflipped. A separate function was used to find m. To obtain the thermal average we took the mean of the observables past equilibrium. For lattice sizes up to $N = 40$, it is sufficient to average past $1000MCs$ (see Section 5.2).

The errors in C and χ' were obtained using the blocking method [10]. Applied to the specific heat, measurements of E were divided into blocks of $100MCs$. Calculating C separately for each block, and

Initial spin state	Flipped spin state	Neighbours	E	ΔE	P_{flip}
$\downarrow$	$\uparrow$	$\downarrow\downarrow\downarrow\downarrow$	-4	8	$\exp\left(\frac{-8}{T}\right)$
$\uparrow$	$\downarrow$	$\downarrow\downarrow\downarrow\downarrow$	$4-$	-8	1
$\downarrow$	$\uparrow$	$\uparrow\downarrow\downarrow\downarrow$	-2	4	$\exp\left(\frac{-4}{T}\right)$
$\uparrow$	$\downarrow$	$\uparrow\downarrow\downarrow\downarrow$	2	-4	1
$\downarrow$	$\uparrow$	$\uparrow\uparrow\downarrow\downarrow$	0	0	1
$\uparrow$	$\downarrow$	$\uparrow\uparrow\downarrow\downarrow$	0	0	1
$\downarrow$	$\uparrow$	$\uparrow\uparrow\uparrow\downarrow$	2	-4	1
$\uparrow$	$\downarrow$	$\uparrow\uparrow\uparrow\downarrow$	-2	4	$\exp\left(\frac{-4}{T}\right)$
$\downarrow$	$\uparrow$	$\uparrow\uparrow\uparrow\uparrow$	4	-8	1
$\uparrow$	$\downarrow$	$\uparrow\uparrow\uparrow\uparrow$	-4	8	$\exp\left(\frac{-8}{T}\right)$

Table 2: The E, ΔE and P_{flip} of a spin with $H = 0$ based on its surrounding neighbours. E and ΔE were calculated using Eq. (1).

the spread of values from one block to another, gave us an estimate of the overall error in C.To obtain $T_c(N)$ from the locations of peaks in χ and C against temperature we

1. Identified ~ 5 data points around the highest value.
2. Plotted a parabola, $y = ax^2 + bx + c$ about these points.
3. Obtained T_c via $T_c(N) = \frac{-b}{2a}$, the turning point of the parabola.

The parabola was plotted using `scipy` library's `optimize.curve_fit` functions, which from errors in C and χ, gave uncertainties for a, b and thus $T_c(N)$. Plotting $T_c(N)$ vs $N^{-1/\nu}$ allowed us to obtain $T_c(\infty)$ and a from the intercept and gradient (assuming the theoretical value of $\nu = 1$ [7]).

The oscillating magnetic field was implemented by sampling

$$H(t) = H_0 \cos(\Omega t) \tag{17}$$

at each MCs, where $\Omega = \frac{2\pi}{t_P}$ with t_P being the discrete time period in MCs.

4 Performance

Two main precautions were taken to improve the performance our programme: reduce the number of computations within `for` loops and avoid recalculating results. Methods utilised to speed-up our programme included

- Avoiding calculating ΔE and $\exp(\frac{-\Delta E}{T})$ every time a lattice site is visited, by instead looking at the spin's nearest neighbours and take the result from Table 2
- Using vectorisation, which provides a speed up over `for` loops, wherever possible [2].
- Calculating E by adding ΔE at each flipped site. This saves us having to visit each lattice site twice: once to propagate the lattice through time and once to calculate the energy of the new state without flipping spins.

Figure 4 illustrates the linear speed-up that implementing these changes has on the Metropolis algorithm. The gradient of the "fast" and "slow" algorithms are 1.92 and 2.00 respectively, and thus $\tau \approx O(n^2)$

Despite this, iterations of the Metropolis algorithm at 30 different temperatures over $100,000 MCs$ with $N = 40$ took several hours.

5 Results and Discussion

5.1 Striped States

Analysing the time for m to reach equilibrium from a disordered input lattice (Figure 6a) at $T << T_C$, we immediately encountered anomalous results. Figure 5 shows the system settling to an equilibrium

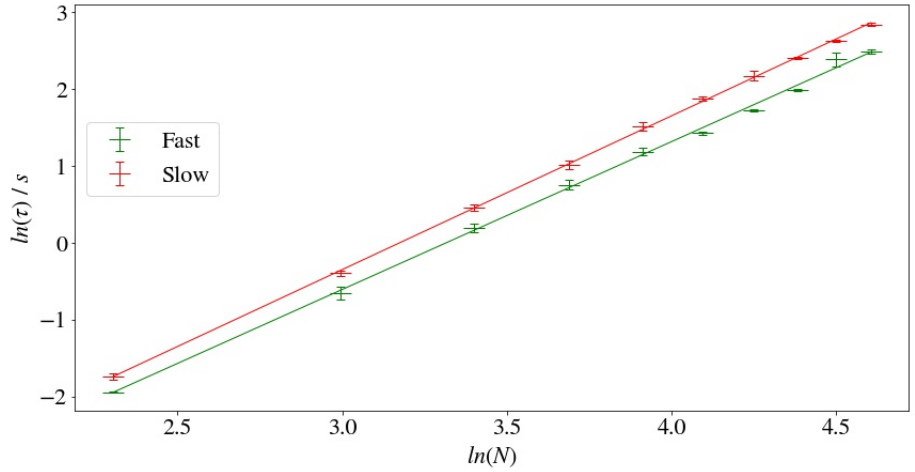

Figure 4: $\ln(\tau)$ against $\ln(N)$, where τ is the time in seconds for the Metropolis Algorithm to run for $100MCs$ at $T = 3$. The green/red lines correspond to algorithms that do/don't use the speed-ups listed in Section 4.

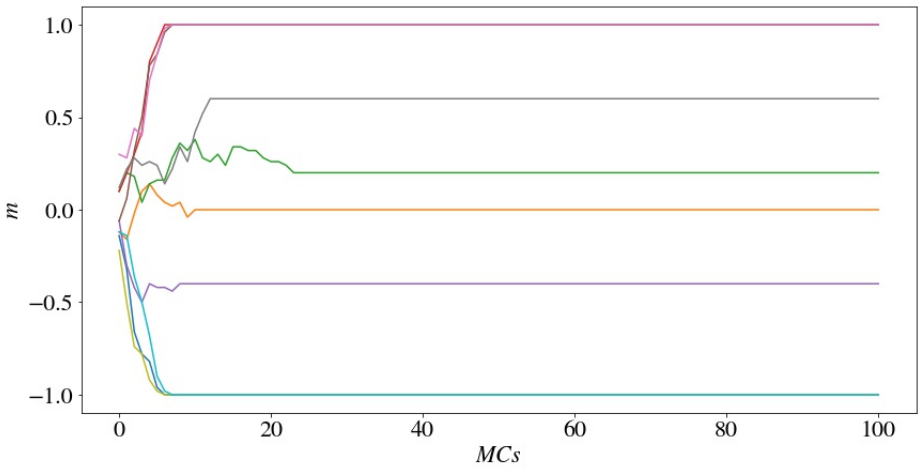

Figure 5: m vs MCs for 10 different disordered input lattices ($N = 10, T = 0$)

value of $m = \pm 1$ with probability $\sim 2/3$. This is expected at $T = 0$; all the spins are aligned, minimizing U and hence F according to Eq. (6). However, there are instances where the system instead develops into to a metastable "striped state", for example in Figure 6b (see *Form sandwich.gif*). Striped states are characterized by alternating horizontal or vertical stripes of homogeneous spins with width ≥ 2. We can see in Figure 6b that each spin in a stripe has at least three neighbours, corresponding to a very small P_{flip} and thus a long lifetime. At $T \to 0$, these metastable states have infinitely long lifetimes [13].

5.1.1 Probability of Forming a Striped State

By calculating the ratio of 100 disordered inputs that developed into a striped states, an estimate probability of forming a striped state as a function of N, $P_{str}(N)$, at $T = 0$ was found. Comparing our results with those in Figure 8 produced by Spirin, Krapivsky, and Redner [13], our data follows a similar trend; at small N, P_{str} rapidly rises until reach a maximum of ~ 0.4 at $N = 15$. Whereas Figure 8 gently decreases in P_{str} past $N = 15$, tending toward $P_{str}(\infty) = 0.3$, we observed a steeper, wider spread descent towards $P_{str}(\infty) = 0.15$. The disparity between Figure 7 and Figure 8 is likely due to the difference in the number of initial configurations used for each N (100 compared to 10^6).

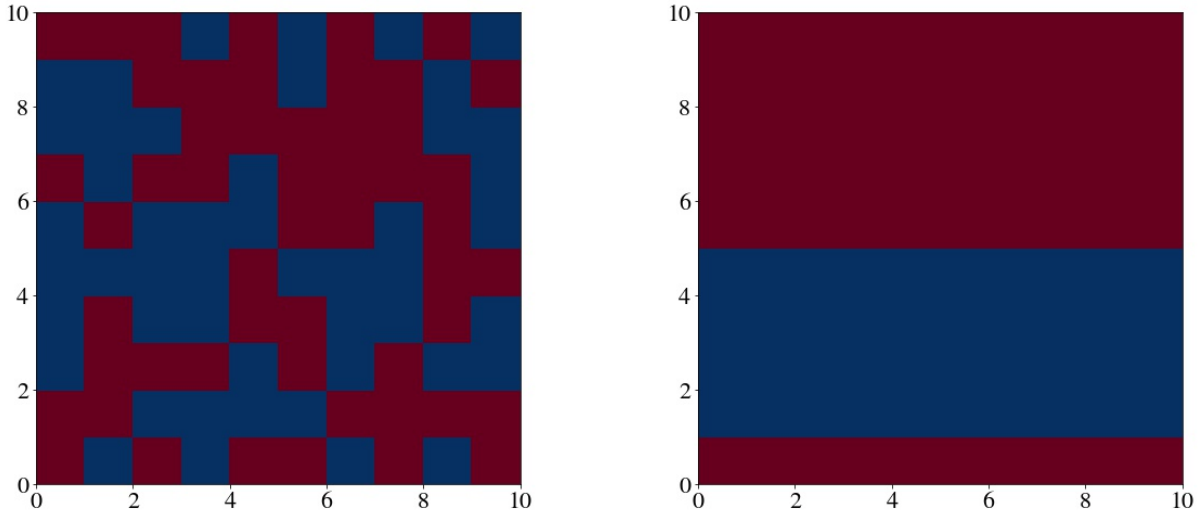

(a) Initially random input lattice

(b) Metastable striped state

Figure 6: Initial and final configurations as a $N = 10$ lattice develops into a striped state

5.1.2 Lifetime

Given our system is in a stripe state, the time to reach a ground state is of order $t_{eq,g} \sim N^3 e^{4/T}$ [14], where the exponential factor is due to the P_{flip} when surrounded by three neighbours of the same spin (Table 2). The gradient of 4.32 for $\ln(t_{eq,g})$ against $1/T$, as in Figure 9, supports this theory.

Including striped states in our time averages resulted in significant deviations from the exact results presented in Section 5.4. Once they appeared at low T, it would not be possible to remove them on a reasonable timescale- for a $N = 20$ lattice at $T = 0.1$, we would require $\sim 10^{21} MCs$ to reach true equilibrium. Furthermore, having a $\sim 1/3$ chance of forming at $N = 512$ [13], which could hold as $N \to \infty$, we cannot simply make the lattice larger.

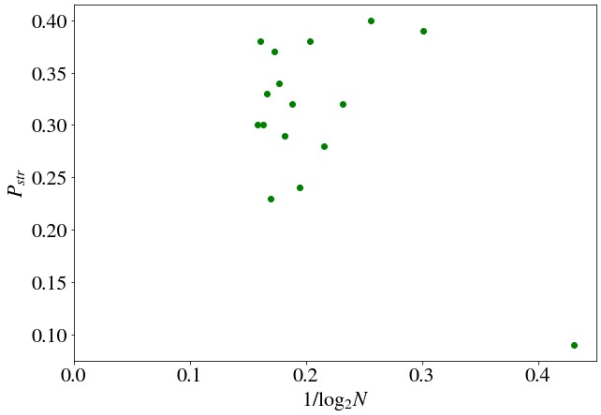

Figure 7: $P_{str}(N)$ vs N for $T = 0$. 100 Initial configuration were used for each N.

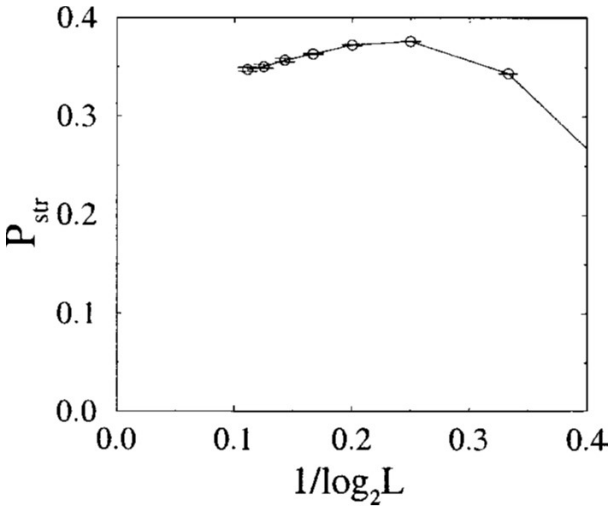

Figure 8: Results for P_{str} vs $1/\log_2(L)$ from [13]. Here $L \leftrightarrow N$, and 10^6 initial configurations were used for each N.

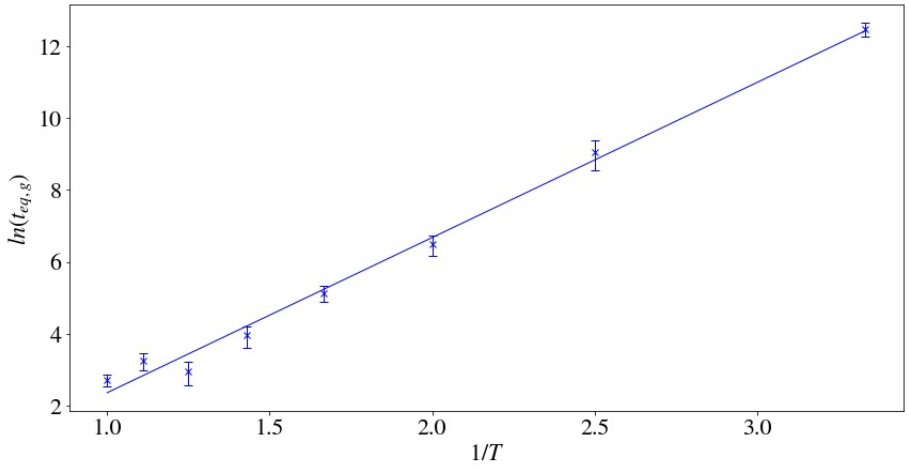

Figure 9: $\ln(t_{eq}, g)$ vs $1/T$, where t_{eq} is measured in No. MCs. A gradient of 4.32 is in rough agreement with the theory that $t_{eq,g} \sim N^3 e^{4/T}$

5.1.3 Solutions

The first attempt to eliminate striped states was to include next-to nearest neighbour interactions within our simulation: if $\Delta E = 0$, instead of flipping the spin as before, we look at the spins diagonal to our selected site and repeat the flipping process. For $N = 10$, a P_{str} of 0.297 ± 0.004 was obtained. Compared to Figure 8, this provides an improvement of ~ 0.05. Whilst this improvement is not significant enough to warrant further use in this case, the implication of increasing the number of interacting neighbours on P_{str} could be interesting for future investigations.

An alternative solution was to slowly quench T when measuring observables. This was achieved by initializing our system with a disordered lattice at high T, and then as we make small decrements in T, the final configuration of the previous T becomes the initial configuration. As we move into the region $T \sim 0.2T_c$, where the relaxation time of striped states is comparable to the zero-temperature system [14], our initial lattice will have $m \geq 0.9$. As energy fluctuations are small in comparison with the energy of the entire system, we expect and observe no striped states to appear [15, 10]. A similar approach would be to instead input a ground state lattice at $T = 0$ and then increment upwards, but this was rejected as it loses the property of symmetry breaking below T_c as the negative values of m are inaccessible. This method has the additional benefit of reducing the No. MCs required to reach equilibrium, as the input lattice is close to the equilibrium lattice.

5.2 Time to Reach Equilibrium

Observing initially disordered configurations elapse over time in Figure 10, it became clear that the No. MCs required to reach equilibrium increases with N. Defining t_{eq} as the number of MCs such that

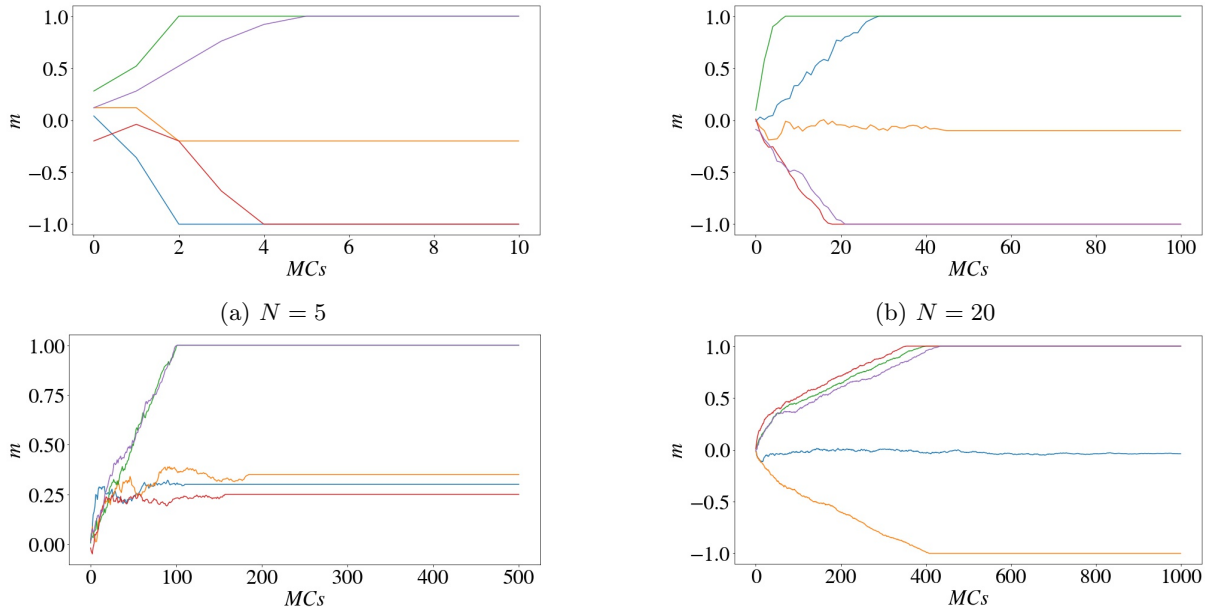

(a) $N = 5$ (b) $N = 20$

(c) $N = 40$ (d) $N = 100$

Figure 10: Evolution of m for varying N at $T = 0.1$

$m \geq \langle m \rangle$, a quantitative analysis of t_{eq} for both a disordered configuration and a striped state at $T = 1.8$ was carried out. The black dashed/dotted lines in Figure 11 suggest that t_{eq} has a quadratic/ cubic dependence for random/ striped initial configuration, which is as expected [8]. The red line, $t_{eq} = 10^3$, lies above all $N \leq 40$. This, in conjunction with the method described in Section 5.1.3, allows us to conclude equilibrium is reached in the first $1000MCs$ for $N \leq 54$, and hence these are removed in our time averages discussed below.

5.3 Auto-covariance

Loosely speaking, the decorrelation time τ_e is a measurement of how long it takes the system to get from one state to another which is significantly different. If we want independent samples, "the most natural

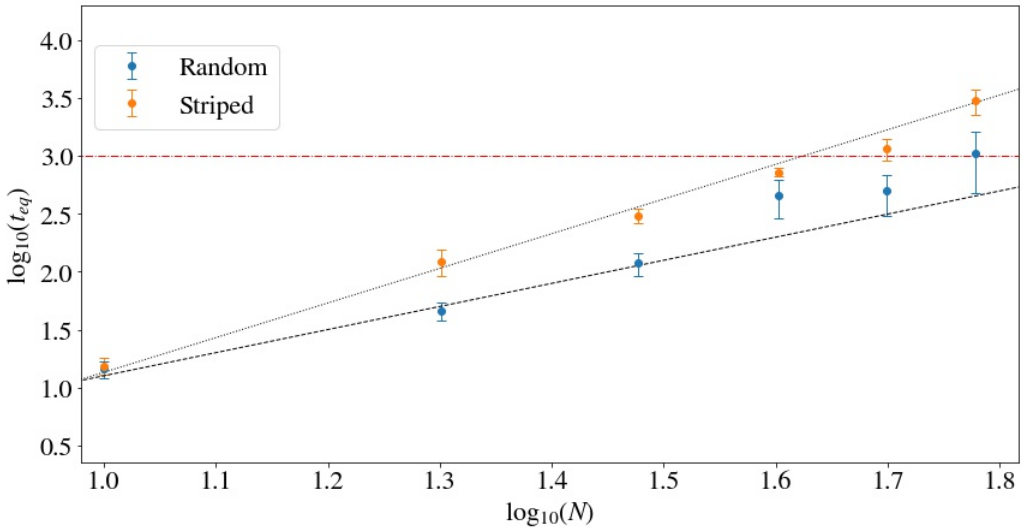

Figure 11: log-log plot of t_{eq} vs N at $T = 1.8$. The black dashed line has gradient of 2, whilst the black dotted line has a gradient of 3. The red dashed line shows $t_{eq} = 10^3$

definition of statistical independence" occurs for sampling intervals of $2\tau_e$ [10]. Thus if a simulation lasts time t_{max} (excluding t_{eq}), then the number of independent measurements possible is

$$n = \frac{t_{max}}{2\tau} \tag{18}$$

The dependence of τ_e against T, is illustrated in Figure 12. At low T, τ_e remains < 10 until it suddenly spikes between $1.7 < T < 2.3$, with the smaller lattices peaking first. These peaks lie close to T_c in the critical region. After $T = 2.5$, τ_e settles down with all N following the same curve.

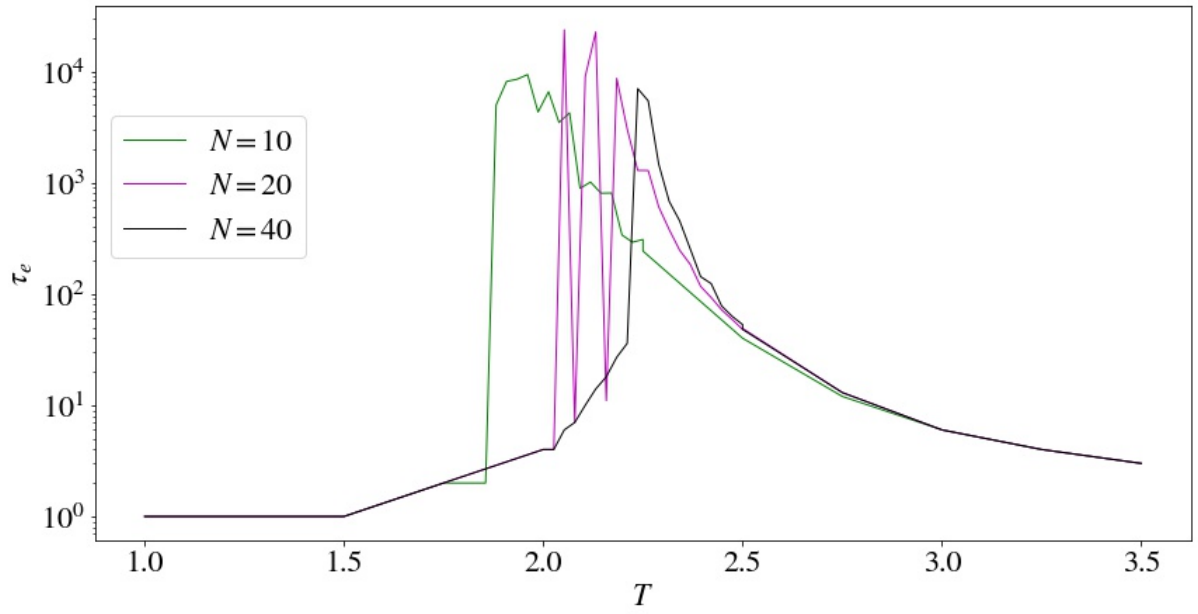

Figure 12: τ_e vs T for $N = 10, 20, 40$. τ_e peaks in the critical region due for all N, with the peaks occurring at hotter T for greater N.

From Figure 13, the system tends to form large clusters of spins around T_c. The state of these spins are strongly correlated- as they flip from one orientation to another, large *critical fluctuations* in m occur, as demonstrated in Figure 14 at $t \approx 20000MCs$. Additionally, the process of flipping a large, correlated cluster of spins is very slow, and thus the fluctuation time diverges at T_c in a process known at *critical slowing down* [1]. The combination of increased fluctuation time and correlation results in the peaks of

τ_e. These effects presents a clear problem within our calculations; if we desire sample a large number of configurations, say 10^4, that are statistically independent according to Eq. (18), the value of $\tau_{e,max}$ for $N = 20$ would require $\sim 4.7 \times 10^8$ sweeps. Based on our current Metropolis algorithm, the time for time to compute this is impractical (Section 4). Although we focus on the Metropolis algorithm, thankfully there are alternatives: the Wolff algorithm, which involves building up clusters of spins which are then flipped together, is much more effective near T_c [1].

Based on this information, how should we sample our observables? If we constrain $t_{max} = 10^6$ and $n = 10^5$, this allows us to have a max sampling interval of $\Delta t_{max} = 5MCs$, which was used in the critical regions shown by Figure 12, with $\Delta t = 1$ everywhere else.

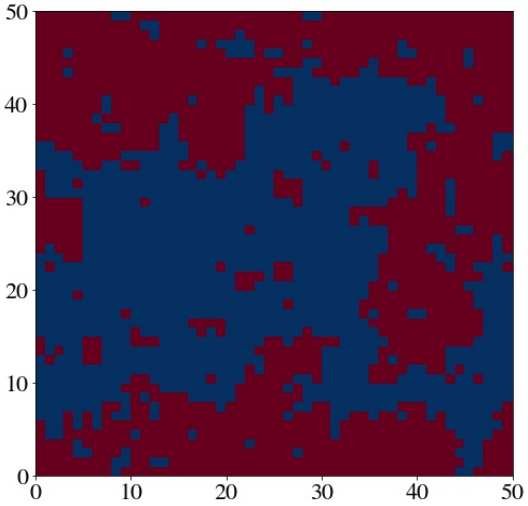

Figure 13: Configuration of a $N = 50$ lattice at $T = 2.25$. Near T_c, large domains of spins can clearly be seen. These cause sizable, infrequent fluctuations in m.

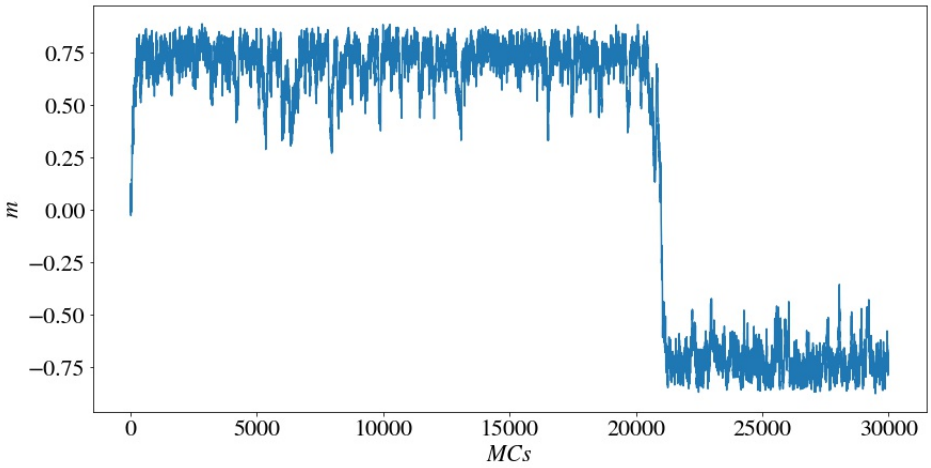

Figure 14: Variation of m with time at $T = 2.25$. At $t \approx 20000MCs$ we observe an example of a large critical fluctuation.

5.4 E vs T

In comparison to the exact result of Eq. (9), the data for E vs T at $N = 2$, as illustrated in Figure 15, strongly agrees and reassures the validity of our simulation. In Figure 16 the energy per spin as a function of temperature for varying N is shown. With increasing lattice size, the curve of the graph becomes more pronounced. However, the curve appears to tend towards the shape given by $N = 40$ (the $N = 20$ (not plotted) and $N = 40$ curves overlap.) This steepening of the gradient gives signs of a phase transition occurring. In the low T limit, all N reach $\langle E \rangle / N^2 = -2$ as expected for completely

aligned spins. In comparison, at higher temperatures, a less negative $\langle E \rangle / N^2$ is observed. This further agrees with Eq. (6)- at higher T disordered configurations that are higher in energy are favoured.

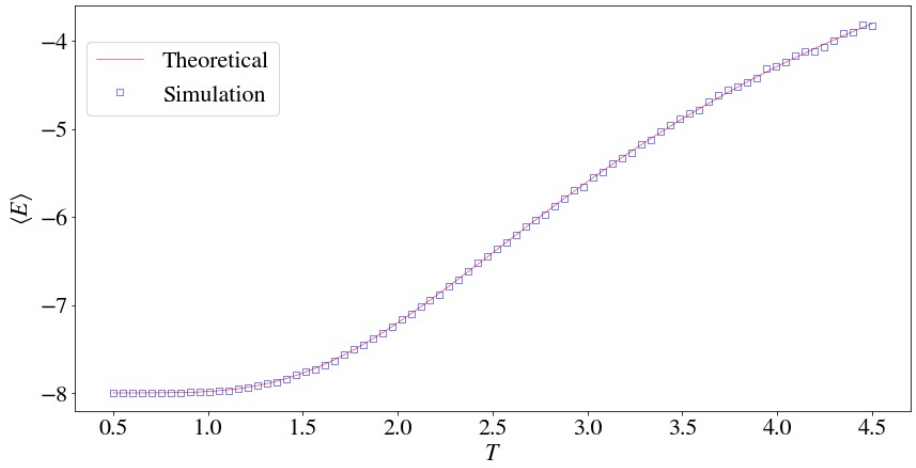

Figure 15: $\langle E \rangle$ vs T for $N = 10$, in comparison to the theoretical result.

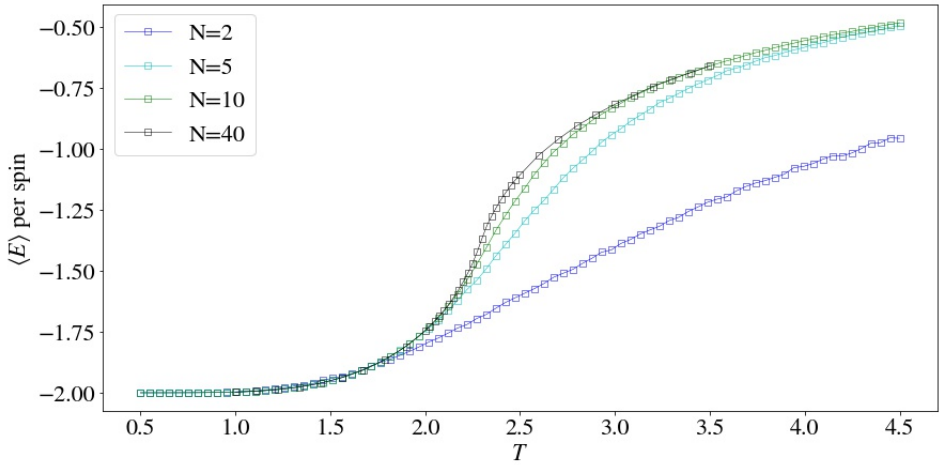

Figure 16: $\langle E \rangle$ per spin vs T for varying N.

5.5 Spontaneous Magnetisation

The results of $|\langle m \rangle|$ vs T suggest behaviour uncharacteristic of the prescribed theory. At $N = 40$, Figure 17a illustrates that $|\langle m \rangle|$ is in good agreement with the theoretical prediction of Eq. (11). However, by decreasing the lattice size, Figure 17b and 17c show $|\langle m \rangle| = 0$ being reached at decreasing T. A peak in the magnetisation's variance and thus the magnetic susceptibility would be present at these apparent "transitions", and Figure 18 confirms this. This approach of the peak in susceptibility towards the curie temperature from the left with increasing N is inconsistent with the theory [3]. It also suggests $T_c(N)$ is lower for decreasing N, which is inconsistent not only our own results, but those of others [6].

The root of this issue arises from the finite probability that all our spins simultaneously flip. In Figure 19, such a flip is seen for a $N = 2$ lattice at $T = 0.8$. This probability is directly proportional to the No. MCs used and inversely proportional to N. Consequentially, $\langle m \rangle$ will average out to zero over long time scales, which is in contrast to what we observe in real systems where spontaneous magnetisation (non-zero magnetisation due to aligned spins at low T) is observed [5]. This behaviour is averted by instead considering $\langle |m| \rangle$ and a modified magnetic susceptibility χ', where

$$\chi' = \frac{\langle M^2 \rangle - \langle |M| \rangle^2}{T} \tag{19}$$

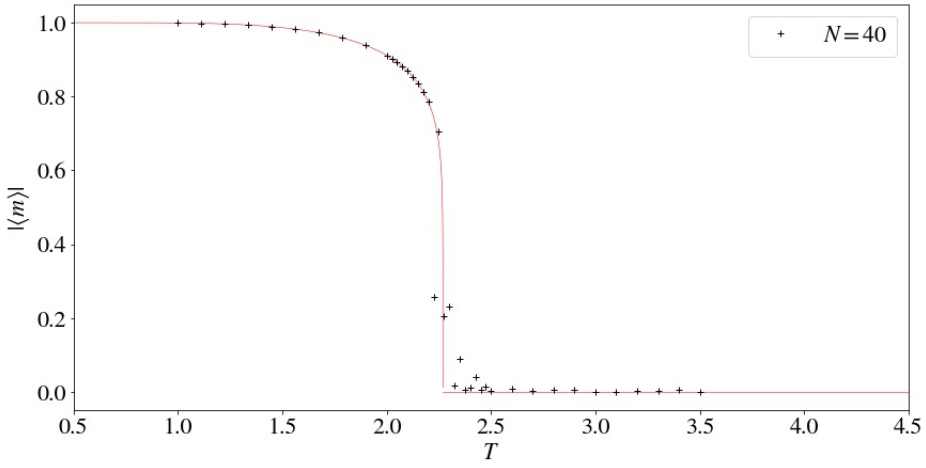

(a)

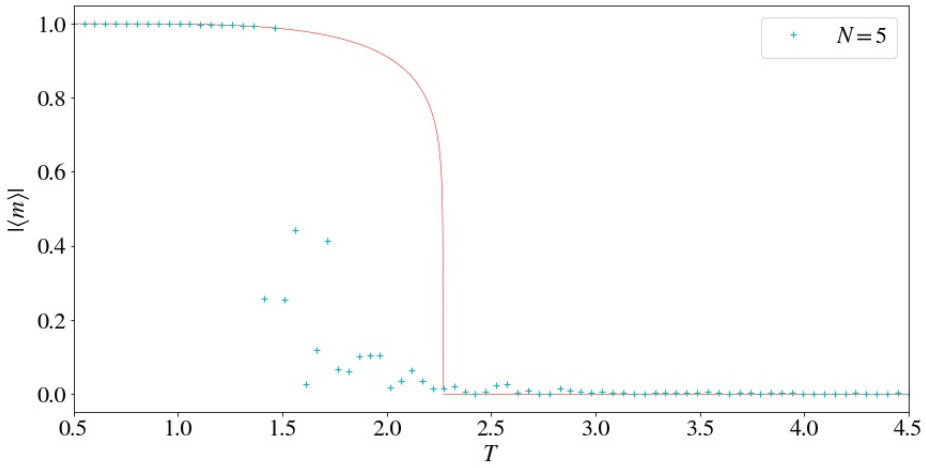

(b)

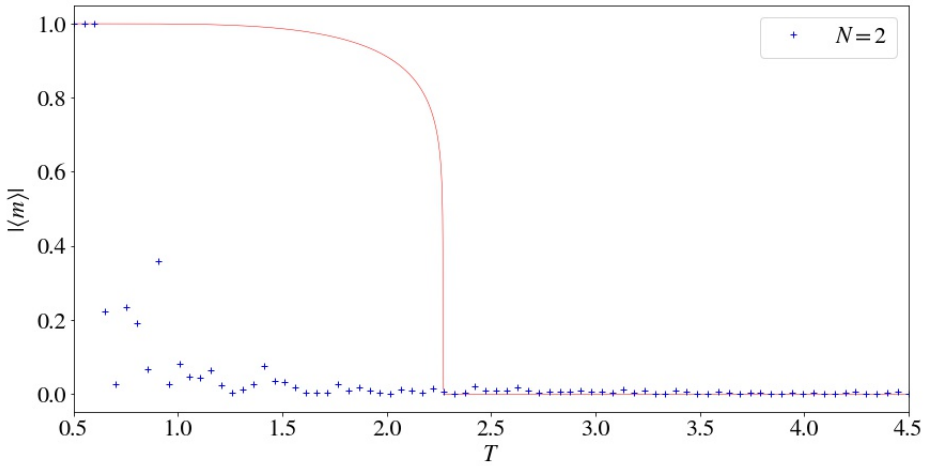

(c)

Figure 17: $|\langle m \rangle|$ vs T for varying N. The red line plotted is Eq. (11), the theoretical function of m as $N \to \infty$. Due to spontaneous magnetisation, the critical point appears to shift to the left with decreasing N, contrary to what we expect.

Although $\langle m \rangle \neq 0$ at high temperatures due to the average of only positive values this is inconsequential as it does not affect the position of the critical point as this effect takes place only for $T > T_c$.

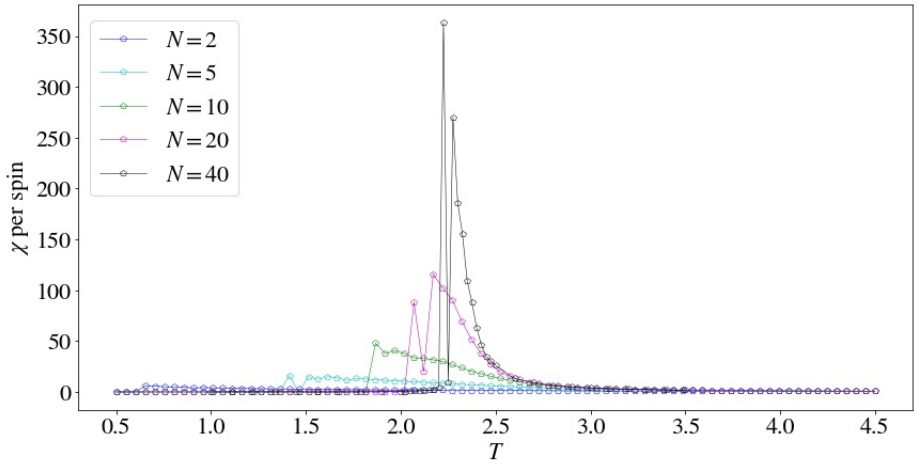

Figure 18: χ per spin vs T for varying N. As we increase N, we see the peak in the susceptibility approach T_c from the left.

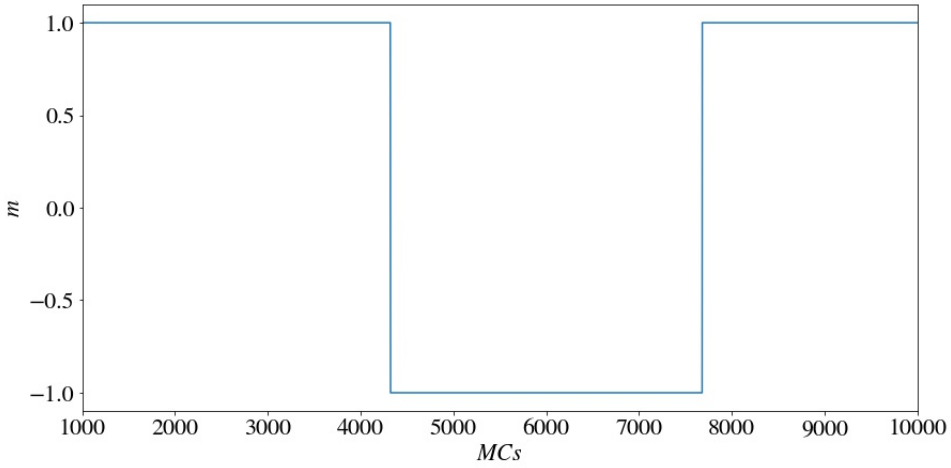

Figure 19: m vs time ($N = 2$, $T = 0.8$). At $\sim 4200MCs$ we see all the spins in the lattice spontaneously flip from $\uparrow$ to $\downarrow$. This spontaneous flipping reoccurs at $\sim 7800MCs$, realigning all the spin upwards again.

5.6 $\langle|m|\rangle$ vs T

From Figure 20, our results for $\langle|m|\rangle$ vs T at $N = 2$ show great agreement with the exact result of Eq. (10). A comparison of $\langle|m|\rangle$ vs T for varying N is illustrated in Figure 21. The distinct change in gradient, becoming more defined with increasing N, signifies that a second-order (continuous) phase transition occurs. This transition through $\langle|m|\rangle$ is far more acute and sensitive to system size than the observation in $\langle E\rangle$. Furthermore, the behaviour of our system is as the theory of Eq. (6) prescribes: unity m at low T due to aligned spins that maximizes U and low m for high T due to a disordered configuration that favours S.

5.7 C, χ' and T_c

Our results of C per spin against T, illustrated in Figure 22, show a broad peak form at $N = 2$ in the critical region. With increasing N, this peak narrows, increases in value and shift towards the left, approaching $T_c(\infty)$. A similar trend is observed for χ' vs T in Figure 23, except for larger N the peaks are more defined. The increase in fluctuations expected about T_c translates into these peaks observed in our plots.

Eq. (12) was plotted in Figure 24 for $T_c(N)$ obtained via C, χ' and an average of the two. A value of $T_c(\infty) = 2.275 \pm 0.006$ was obtained from the intercept and is in agreement with Onsager's exact

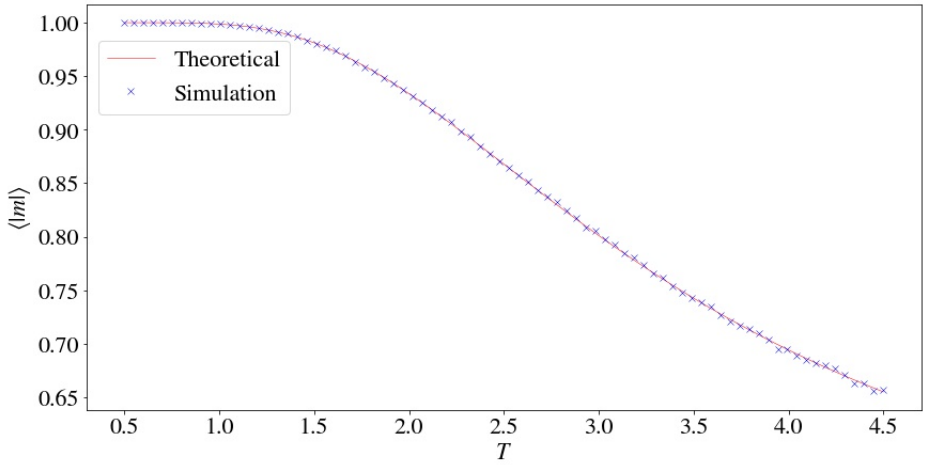

Figure 20: $\langle|m|\rangle$ vs T at $N = 2$. Our data is compared to the exact result of Eq. (10).

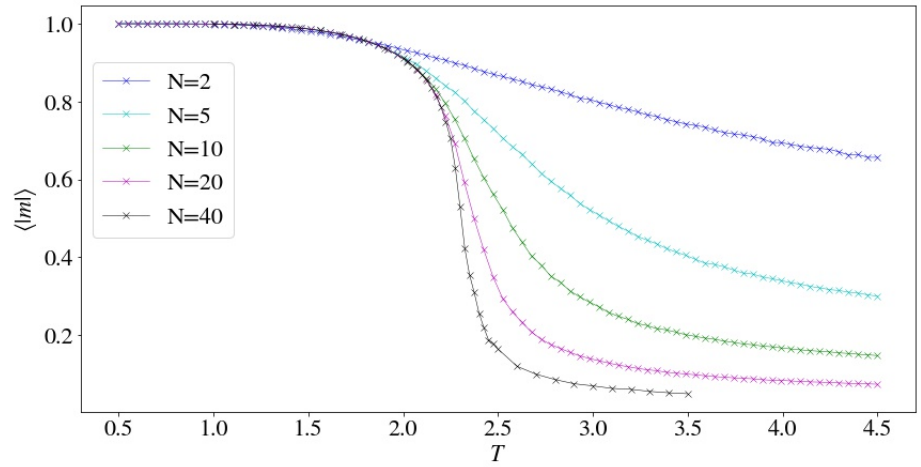

Figure 21: $\langle m\rangle$ vs T for varying N. The steep change in gradient signifies that a phase transition has occurred. This is more prominent for larger N

result of $T_c = \frac{2}{\ln(1+\sqrt{2})} \approx 2.269$. Considering only χ'/C data led to values of $T_{c,\chi}(\infty) = 2.268 \pm 0.003$ and $T_{c,C}(\infty) = 2.284 \pm 0.01$. A Less precise and accurate value of T_c was found from using the C data relative to the χ' data, due to the broader peaks exhibited when plotted against temperature. A gradient of $a = 1.28 \pm 0.06$, calculated by an average of $a_\chi = 2.08 \pm 0.05$ and $a_C = 0.49 \pm 0.13$. The lower precision observed in our C data compared to χ' is likely due to the peaks being less defined, which result from our $\langle E\rangle$ curves being shallower than those for $\langle|m|\rangle$ results

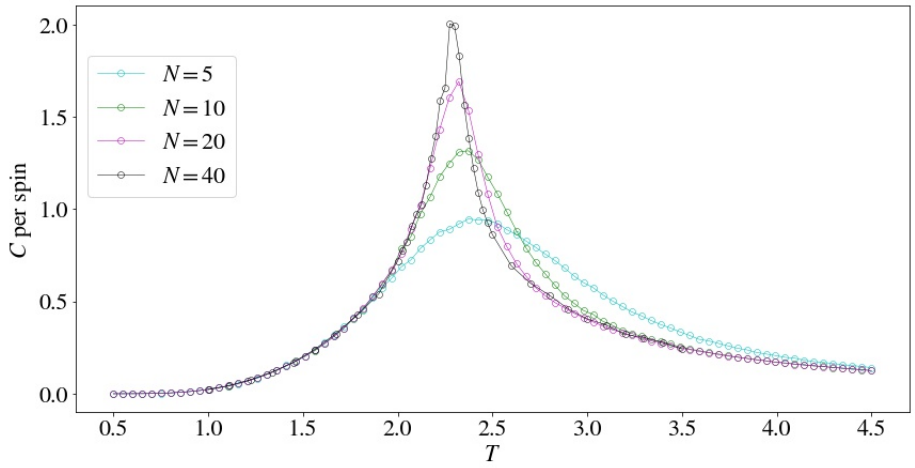

Figure 22: C per spin vs T for varying N. Peaks on the graph correspond to fluctuation of the energy at the critical point. As N increases, the peaks become narrower, shift to the left and increase in value.

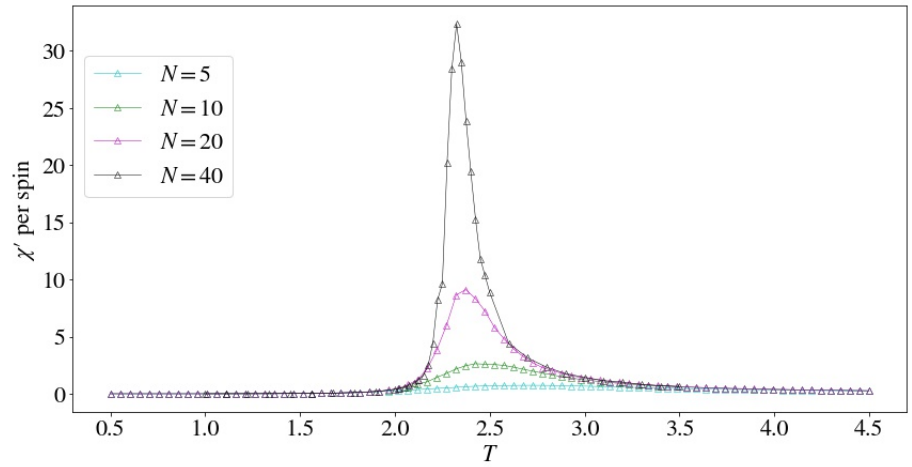

Figure 23: χ' per spin vs T for varying N. Peaks on the graph correspond to fluctuation of $\langle m \rangle$ at the critical point. As N increases, the peaks become narrower, shift to the left and show a large increase in value.

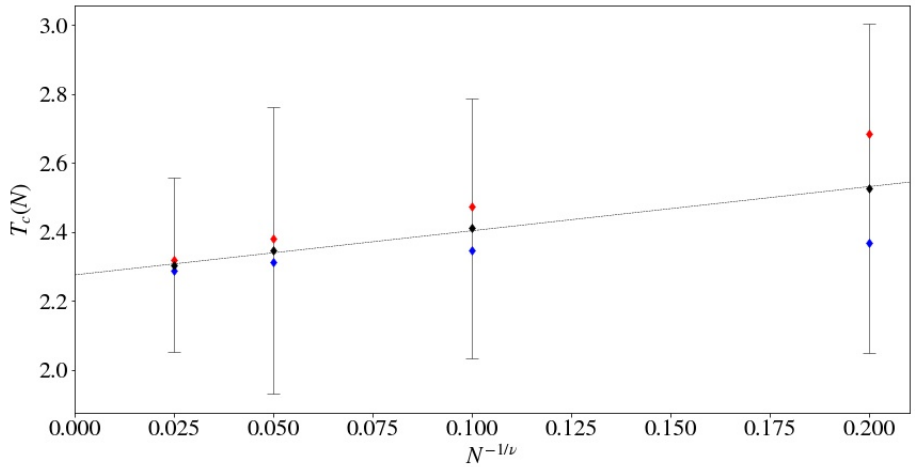

Figure 24: $T_c(N)$ against $N^{-1/\nu}$. The red/blue points correspond to data obtained from peaks in the χ'/C data. The black points in an average of the two, and its error bars are shown.

5.8 Magnetic Field

The time period of oscillation was fixed at $t_P = 100MCs$, whilst the temperature was varied in the range $0.5 \leq T \leq 5$ for $H_0 = 1, 10$. In the $H_0 = 1$ regime, the hysteresis loops went through a number of shapes with increasing T. At the lowest temperatures, m remained at 1 as H fluctuated. An example of this is shown in Figure **??**, and is observed do to the fast that H isn't strong enough to overcome the decrease in energy from having spins aligned, i.e. $\Delta E > 0$ for all values of H. For higher T, the loop

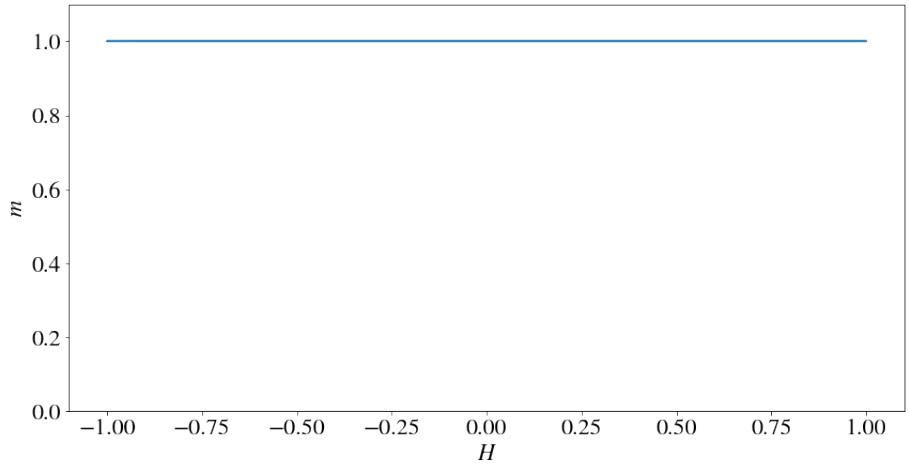

Figure 25: m vs H $(T = 0.5, H_0 = 1)$. m retains a constant value of 1 for varying H

moves through an asymmetric ellipse, where the major axis is inclined with respect to the H axis (Figure 26), into a standard hysteresis shaped loop (Figure 27) which has a large remnant magnetisation and coercive field.

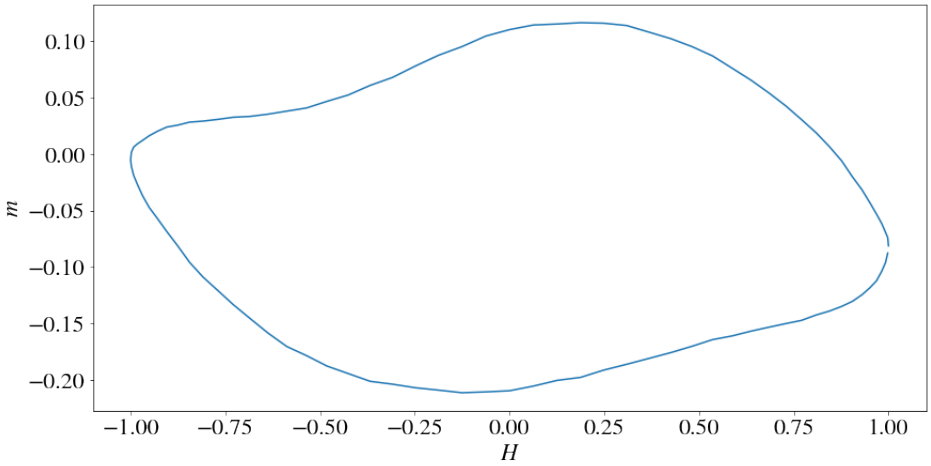

Figure 26: m vs H $(T = 0.97, H_0 = 1)$. The hysteresis loop has a distorted, elliptical shape, with its axis aligned to the H axis at an angle

As T is further increased, we observe in Figure 28 a decrease in the coercive field, loop area, remnant magnetisation and saturation. This process occurs until Figure 29 where the area reaches zero and we obtain a linear response with no remnant magnetisation or coercive field. With increasing T, thermal fluctuations of the m increase, which hasten the decay of a metastable state and thus decrease the coercive field [12].

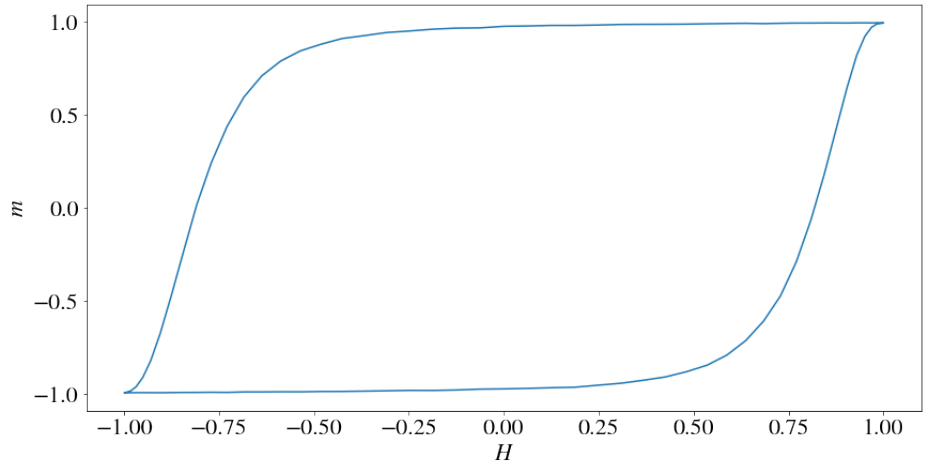

Figure 27: m vs H $(T = 1.45, H_0 = 1)$. The hysteresis loop has its standard shape

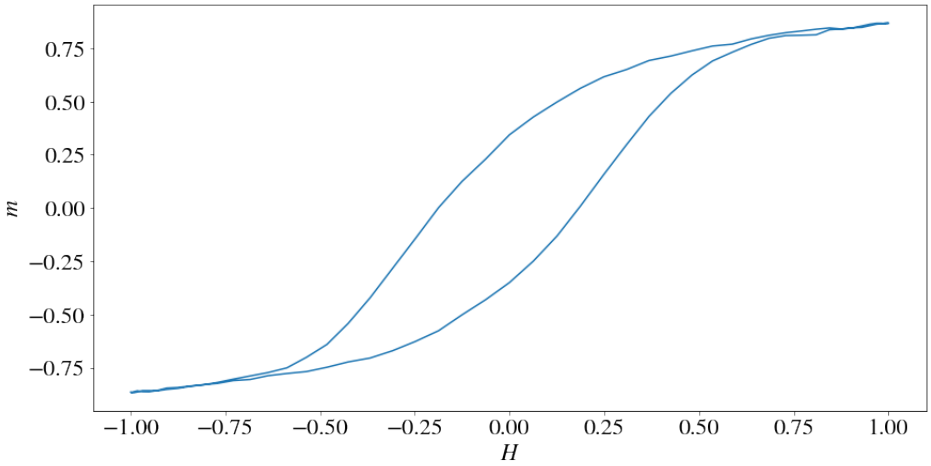

Figure 28: m vs H $(T = 3.11, H_0 = 1)$. The coercive field, remnant magnetisation and saturation begin to decrease.

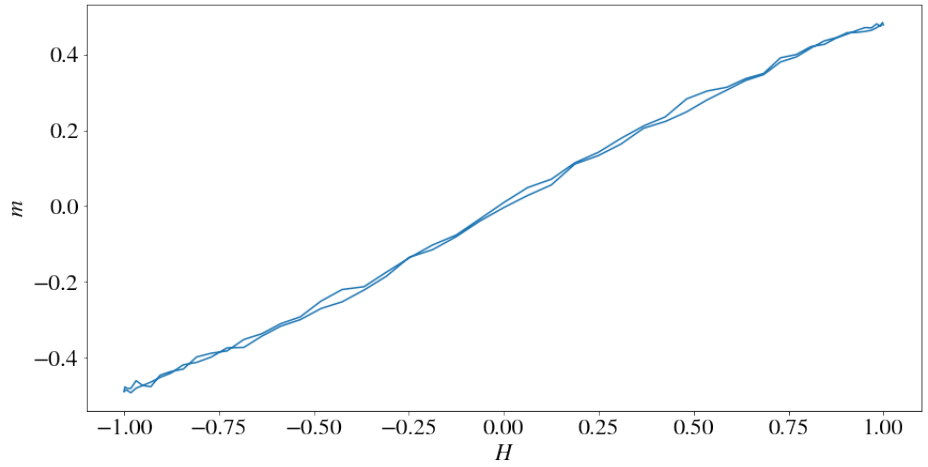

Figure 29: m vs H $(T = 5, H_0 = 1)$. m has a linear response to H

In the case of $H_0 = 10$, the standard hysteresis loop shape was seen for low T in Figure 30. Increasing T, the overall shape was kept the same except for decreasing the coercive field and area. In the high T limit, the coercive field and area reduce so zero, as observed in Figure 31, but the saturation remained unaffected Loop area against T for $H_0 = 1, 10$ is plotted in Figure 32

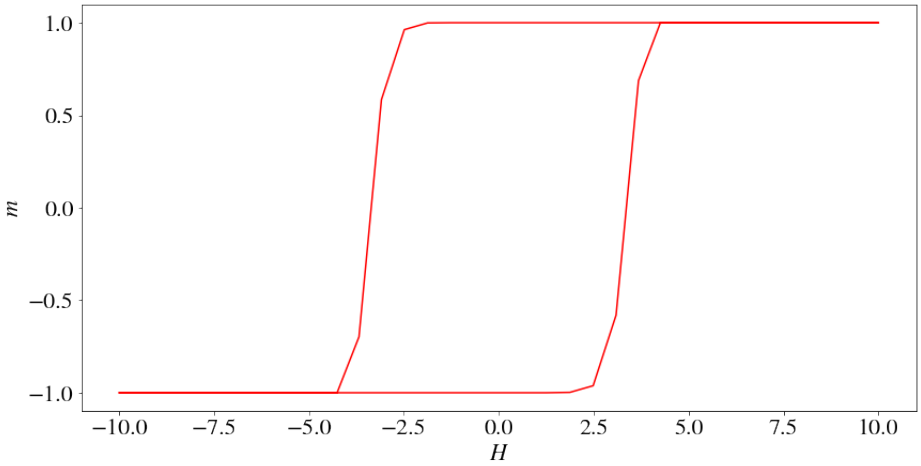

Figure 30: m vs H $(T = 0.5, H_0 = 10)$. At low T, the standard hysteresis loop shape is seen.

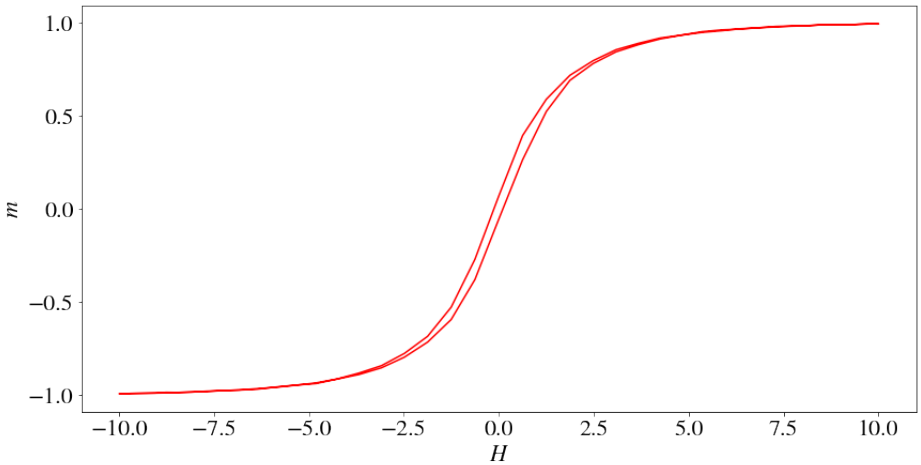

Figure 31: m vs H $(T = 0.5, H_0 = 10)$. At high T, the loop area and coercive field reduce to zero, but the saturation is unaffected.

For $H_0 = 1$ and low values T, the loop area remains small until there is an abrupt change for the loop area at $T = 1.2$, indicating a phase transition. After this point, the area of the loop decreases exponentially with T. The $H_0 = 10$ curve exhibits exponential decay with T and maintains a higher high loop area than $H_0 = 1$ for all values of T, corresponding to a larger energy dissipation. In the low T limit, the loop area remains high and we don't observe a sudden change in area. Due to the large field strength, the spins follow the direction of the field. Whereas with $H_0 = 1$, even if the field is aligned opposite to the spins, it cannot overcome the interaction energy of the aligned lattice and ΔE remains positive.

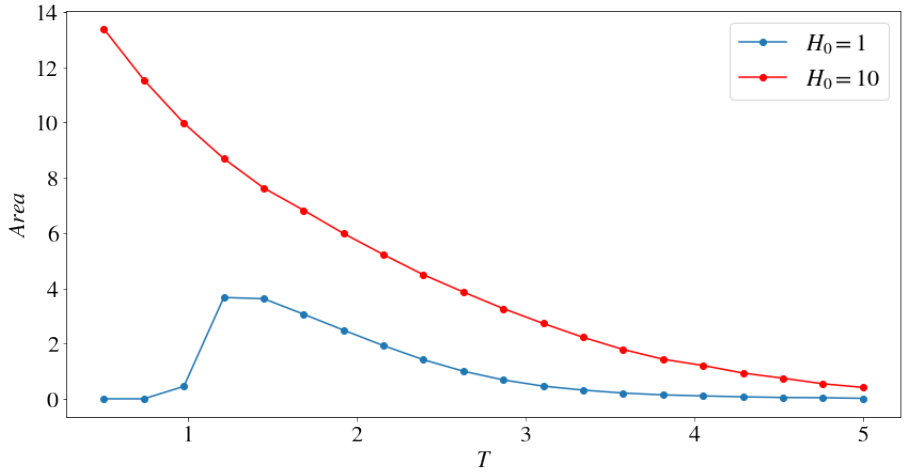

Figure 32: Area of hysteresis loop vs T for $H_0 = 1, 10$. In both cases, the area exponentially decays with T, except for at $T \sim 1.2$, $H_0 = 1$, where the area suddenly drops to zero.

6 Conclusions

We have implemented the 2D Ising Model for a ferromagnet via the Metropolis algorithm and demonstrated a clear phase transition in our observations of the magnetisation. The critical temperature at which this for varying lattice sizes were found, and by a finite scaling relation, the critical temperature for an infinitely sized lattice was found to be $T_c = 2.275 \pm 0.006$. This result is in agreement with Onsager's theoretical value of $T_c = \frac{2}{\ln(1+\sqrt{2})} \approx 2.269$. The constant a in the finite scaling relation was found to be $a = 1.28 \pm 0.06$. In the low T limit, metastable striped states were observed with probability $\sim 1/3$ and their lifetimes were found in agreement with the theory. These presented a barrier in averaging our observables and were overcome by slowly quenching T from high to low values. Applying an oscillating magnetic field, we observed hysteresis. In general, the coercive field and loop area decreased with increasing T, the loop area exponentially so. For the larger amplitude, T appeared to have no effect on the saturation, as opposed to the weaker amplitude. For $H_0 = 1$ at $T \sim 1.2$, a phase transition was observed where loop area abruptly decreased to zero, and m remained constant at 1 i.e. in its ground state. The phenomena of critical slowing down resulted in large areas around the critical region- the very large decorrelation time we could not take completely independent samples. An advancement on this would be to use an alternative to the Metropolis algorithm such as the Wolff algorithm which performs better in these regions.

References

[1] S. Blundell and K. Blundell. *Concepts in Thermal Physics*. second edition. Oxford University Press, 2010.

[2] David Buscher. *Computational Physics*. Course handout: Department of Physics, University of Cambridge. 2021.

[3] John Cardy. *Scaling and Renormalization in Statistical Physics*. Cambridge Lecture Notes in Physics. Cambridge University Press, 1996. DOI: 10.1017/CBO9781316036440.

[4] Matthias Elf et al. "Branch-and-Cut Algorithms for Combinatorial Optimization and Their Implementation in ABACUS". In: vol. 2241. Jan. 2001, pp. 157–222. ISBN: 978-3-540-42877-0. DOI: 10.1007/3-540-45586-8_5.

[5] F. Malte Grosche. *Thermal and Statistical Physics*. Course handout: Department of Physics, University of Cambridge. 2020.

[6] Jacques Kotze. *Introduction to Monte Carlo methods for an Ising Model of a Ferromagnet*. 2008. arXiv: 0803.0217 [cond-mat.stat-mech].

[7] B. Kutlu. "Critical exponents of the two-dimensional Ising model with next-nearest-neighbor and four-spin interactions on the Creutz cellular automaton". In: *Physica A: Statistical Mechanics and its Applications* 243.1 (1997), pp. 199–212. ISSN: 0378-4371. DOI: https://doi.org/10.1016/S0378-4371(97)00255-0. URL: https://www.sciencedirect.com/science/article/pii/S0378437197002550.

[8] Adam Lipowski. "Anomalous phase-ordering kinetics in the Ising model". In: *Physica A: Statistical Mechanics and its Applications* 268.1 (1999), pp. 6–13. ISSN: 0378-4371. DOI: https://doi.org/10.1016/S0378-4371(99)00005-9. URL: https://www.sciencedirect.com/science/article/pii/S0378437199000059.

[9] Elliott W. Montroll, Renfrey B. Potts, and John C. Ward. "Correlations and Spontaneous Magnetization of the Two-Dimensional Ising Model". In: *Journal of Mathematical Physics* 4.2 (1963), pp. 308–322. DOI: 10.1063/1.1703955. eprint: https://doi.org/10.1063/1.1703955. URL: https://doi.org/10.1063/1.1703955.

[10] M.E.J. Newman and G.T. Barkema. *Monte Carlo Methods in Statistical Physics*. Oxford University Press, 1999.

[11] Lars Onsager. "Crystal Statistics. I. A Two-Dimensional Model with an Order-Disorder Transition". In: *Phys. Rev.* 65 (3-4 Feb. 1944), pp. 117–149. DOI: 10.1103/PhysRev.65.117. URL: https://link.aps.org/doi/10.1103/PhysRev.65.117.

[12] Madan Rao, H. R. Krishnamurthy, and Rahul Pandit. "Magnetic hysteresis in two model spin systems". In: *Phys. Rev. B* 42 (1 July 1990), pp. 856–884. DOI: 10.1103/PhysRevB.42.856. URL: https://link.aps.org/doi/10.1103/PhysRevB.42.856.

[13] V. Spirin, P. L. Krapivsky, and S. Redner. "Fate of zero-temperature Ising ferromagnets". In: *Physical Review E* 63.3 (Feb. 2001). ISSN: 1095-3787. DOI: 10.1103/physreve.63.036118. URL: http://dx.doi.org/10.1103/PhysRevE.63.036118.

[14] V. Spirin, P.L. Krapivsky, and S. Redner. "Freezing in Ising ferromagnets". In: *Physical Review E* 65.1 (Dec. 2001). ISSN: 1095-3787. DOI: 10.1103/physreve.65.016119. URL: http://dx.doi.org/10.1103/PhysRevE.65.016119.

[15] Palani Sundaramurthy and Daniel Stein. "Zero Temperature Dynamics of 2D and 3D Ising Ferromagnets". In: *Journal of Physics A General Physics* 38 (Nov. 2004). DOI: 10.1088/0305-4470/38/2/005.

[16] Sascha Wald. "Thermalisation and Relaxation of Quantum Systems". PhD thesis. Sept. 2017. DOI: 10.13140/RG.2.2.25169.63842.